ON SELF-EXCITED VIBRATIONS DUE TO SLIDING FRICTION IN SYSTEMS OF DEFORMABLE BODIES – GENERAL FORMULATION AND INFLUENCE OF CONTACT PROPERTIES –

Hartmut Hetzler

Institut für Technische Mechanik
Universität Karlsruhe (TH)
KIT – Karlsruhe Institut of Technology
e-mail: hartmut.hetzler@kit.edu

Keywords: Self excitation, friction induced vibration, moving continua, contact, tribology, penalty formulation, constitutive contact modell, surface topography

Abstract. *This contribution presents a generalized approach to friction induced vibrations in systems of moving continua. To this end, Hamilton's Principle is used to state a weak formulation of the system dynamics without using specific structural models, like beams or plates for instance. The normal contact is enforced by a penalty formulation, which motivates the use of a constitutive contact model based on meso- and micromechanical properties.*

By linearization about a stationary solution the perturbation equations are derived in a weak form. Since moving continua are considered, inevitably there will be gyroscopic contributions to the system. Special attention is paid to the derivation and linearization of the frictional contributions. The resulting terms are interpreted with respect to their physical meaning, definiteness and symmetry. It is shown that frictional effects affect the system's stiffness as well as its damping. It is found that using this quite general approach some universal properties can be formulated. Finally, by means of a Ritz-type ansatz a discretization is carried out, leading to a matrix differential equation. Due to stationarity of the considered solution, the differential operators and thus the matrices are time constant.

Furthermore, a simple constitutive contact law following the assumptions of Greenwood-Williamson is stated. It is found, that the contact stiffness is related to the local contact pressure as well as to statistical parameters of the surface topography.

Finally, above results are demonstrated using the example of a rotating Euler-Bernoulli-ring, which is sliding through frictional guidings. First, the general stability of the steady state is discussed. It is found that this steady state may become unstable due to flutter and that the stability behaviour is extremely sensible against damping and gyroscopic effects. Moreover, the influence of tribological contact parameters as the RMS of the asperity heights as well as the contact pressure is demonstrated.

1 INTRODUCTION

Self-excited vibrations in systems of moving elastic bodies are a common phenomenon in engineering applications. Popular examples reach from squealing vehicle brakes or clutches to insufficiently lubricated bearings.
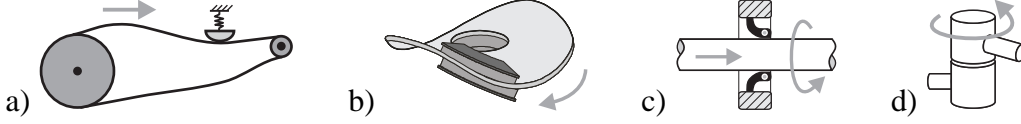
Figure 1: Exemplary systems from engineering application which may show vibrations due to friction self-excitation.

Mostly, it is found that squealing is caused by a flutter-type instability due to friction of the steady-state, which leads to self-excited vibrations. This instability mainly arises from non-conservative contributions of the friction, which – after linearization and discretization – yield a non-symmetric stiffness matrix. In the recent decades, the knowledge about friction induced flutter has steadily grown and was mainly promoted in the context of squealing vehicle brakes. Here, flutter has been known as mechanism since the 1970s [8], but it was not before the beginning of this century, that the influence of the friction onto the system's damping had been revealed [11]. Later, the importance of gyroscopic terms due to the transport motion has been pointed out ([1] for instance), which give rise to gyroscopic-circulatory perturbation equations, that are known to exhibit a complex stability behaviour (e.g. [1], [9], [2]).

Moreover, another mechanism often associated with friction induced vibrations is instability by divergence due to a negative slope of the coefficient of friction. Although the relevance of this mechanism to practical problems is under debate, this model is often used to explain friction induced vibrations [3].

Since usually the above mentioned phenomena are investigated using minimal models, it seems interesting to carry out a general examination – without relying to special assumptions or structural models – in order to clarify, whether there might be further mechanisms and to promote a more global unterstanding.

2 MODELING

In the following, the dynamics of systems of moving elastic bodies with frictional contacts will be described and the perturbation equations of a steady-state solution will be derived. Thereby, the focus will be on general properties of symmetry and definiteness of the resulting differential operators.

2.1 System of moving bodies

In many engineering applications, the stationary motion of an elastic body i may be decomposed into a prescribed rigid body motion $\vec{r}_{Ti}$ and small motions $\vec{w}_i$ about this transport motion, i.e. $\vec{r}_i = \vec{r}_{Ti} + \vec{w}_i$ (cf. fig. 2 a). In the sense of a linearized description, the contact zone Γ_C often may be described with respect to the intermediate configuration $\vec{r}_{Ti}$ after the rigid body motion.

Thus, from $\vec{r}_{Ti}(\mathbf{x}, t) = \vec{r}_{Ti}(\mathbf{X}(\mathbf{x}, t), t)$ follows the identification $\mathbf{x} = \mathbf{X}(\mathbf{x}, t)$, which relates the spatial coordinates $\mathbf{x} = (x, y, z)^\top$ of the intermediate configuration to the corresponding material coodinates $\mathbf{X} = (X, Y, Z)^\top$. If the intermediate configuration and the material reference coincide at $t = 0$, spatial and material coordinates are usually related by $\mathbf{x} = \mathbf{X} + \int_0^t \mathbf{v}_T \mathrm{d}t$, thus $\dot{\mathbf{x}} = \dot{\mathbf{X}} + \mathbf{v}_T$, where $\mathbf{v}_T = (v_{Tx}, v_{Ty}, v_{Tz})^\top$. Please note that the vector fields $\vec{r}_\alpha = \vec{r}_\alpha(\mathbf{x}, t)$ are

adressed by the spatial coordinate $\mathbf{x}$ and thus, material time derivatives $\frac{\mathrm{d}}{\mathrm{d}t}\big|_{\mathbf{X}}$ for fixed $\mathbf{X} = \mathrm{const}$ must account for the transport motion. Consequently, for instance, the field of material velocity reads $\vec{v}_\alpha = \frac{\mathrm{d}}{\mathrm{d}t}\big|_{\mathbf{X}} \vec{r}_\alpha = \dot{\vec{r}} + \mathbf{v}_{T\alpha}^\top \frac{\partial}{\partial \mathbf{x}} \vec{r}_\alpha$ ($\alpha = i, j$).
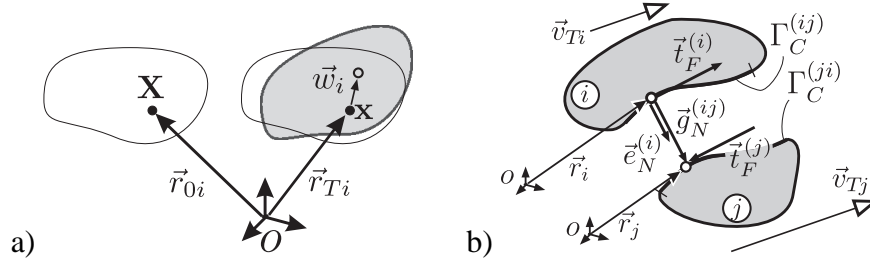
Figure 2: a) Kinematics of a moving deformable body with intermediate configuration after the transport motion. b) Kinematics of the contact between body i and j.

For a system of N bodies, evaluation of an analytical principle, like Hamilton's Principle for instance, and subtracting the steady state due to the transport motion yields a weak formulation of the perturbation equations

$$0 = \sum_{i=1}^{N} \int_{\Omega_i} \delta\vec{w}_i \cdot \left(\mathcal{M}_i[\ddot{\vec{w}}_i] + \mathcal{P}_i[\dot{\vec{w}}_i] + \mathcal{Q}_i[\vec{w}_i] \right) \mathrm{d}v + \Delta\{\delta\Pi_C\} - \Delta\{\delta W_C\} - \Delta\{\delta W_{np}\} \quad (1)$$

where $\Delta\{\}$ denotes linearization, $\mathcal{M}_i = \mathcal{M}_i^\top$ is the mass operator of the ith body and $\mathcal{P}_i = \mathcal{D}_i + v_T \mathcal{G}_i$ contains the symmetric damping operator $\mathcal{D}_i = \mathcal{D}_i^\top$ as well as the skew-symmetric gyroscopic contributions $\mathcal{G}_i = -\mathcal{G}_i^\top$. Moreover, $\mathcal{Q}_i = \mathcal{K}_i + v_T \mathcal{N}_i + v_T^2 \mathcal{K}_i^*$ consists of the symmetric stiffness operator $\mathcal{K}_i = \mathcal{K}_i^\top$, the symmetric centrifugal effects $\mathcal{K}_i^* = \mathcal{K}_i^{*\top}$ and may exhibit skew-symmetric influences $\mathcal{N}_i = -\mathcal{N}_i^\top$ from internal damping. $\Delta\{\delta W_{np}\}$ gathers the virtual work of the remaining non-potential forces, that have not been considered otherwise. In particular, this addend may account for momtentum flux across the system border if open systems are discussed [7].

2.2   Contact

In order to express the contributions of the contact $\Gamma_C^{(ij)}$ between body i and j, the gap vector $\vec{g}^{(ij)} = \vec{r}_j - \vec{r}_i$ is introduced, which connects a surface point on i to its mating contact partner on j. Using the decomposition of the positional field, the gap vector reads

$$\vec{g}^{(ij)} = (\vec{r}_j - \vec{r}_i) + (\vec{w}_j - \vec{w}_i) = \vec{g}_0 + \Delta\vec{g} \quad (2)$$

and thus $\delta(\Delta g_N) = \delta g_N$ holds. On each contact partner, a tangential coordinate frame may be defined using the outward surface normal $\vec{e}_N^{(i)/(j)}$. Using this, the normal gap $g_N^{(ij)}$ is given by $g_N^{(ij)} = \vec{g}^{(ij)} \cdot \vec{e}_N^{(i)}$ and its variation reads $\delta g_N^{(ij)} = \delta\vec{g}^{(ij)} \cdot \vec{e}_N^{(i)}$. The direction of the sliding friction tractions on body i and j read

$$\vec{e}_F^{(i)} = -\vec{e}_F^{(j)} = \vec{v}_{rel}^{(ij)} / |\vec{v}_{rel}^{(ij)}| \quad \text{where} \quad \vec{v}_{rel}^{(ij)} = \vec{v}_j - \vec{v}_i. \quad (3)$$

For the sake of brevity, the superscript (ij) is dropped in the following and the tangential system of body i is used, i.e. $\vec{e}_N = \vec{e}_N^{(i)}$ within a contact (ij).

Using a penalty approach, one may introduce the contact potential $\Pi_C = \frac{1}{2} \int_{\Gamma_C} k_C \langle g_N \rangle^2 \, da$, where $\langle \cdot \rangle = \min(0, \cdot)$ are the so-called McCauley-brackets. Variation and linearization yields

$$\Delta\{\delta\Pi_C\} = \int_{\Gamma_C} \delta g_N \, k_C \Delta g_N \, da, \tag{4}$$

where $p = p(\Delta g_N) \approx p_0 + k_C(-\Delta g_N) = p_0 + k_C(-\vec{e}_N \cdot \Delta\vec{g})$ is the linearized contact pressure and $k_C = \frac{\partial p}{\partial \Delta g_N}|_0$ is the linear contact stiffness, i.e. the linearization of constitutive contact law $p = p(g_N)$ at the working point. Thus,

$$\Delta\{\delta\Pi_C\} = \sum_{(ij)}^{n_C} \int_{\Gamma_C^{(ij)}} \delta\vec{g} \cdot \left[k_C \left(\vec{e}_N \otimes \vec{e}_N\right) \right]_0 \Delta\vec{g} \, da = \sum_{(ij)}^{n_C} \int_{\Gamma_C^{(ij)}} \delta\vec{g} \cdot \mathcal{C}\left[\Delta\vec{g}\right] da, \tag{5}$$

where $\Delta\vec{g} = \vec{w}_j - \vec{w}_i$ and $[\ldots]_0$ stresses that the bracketed terms refer to the linearization point. The symmetric contact stiffness $\mathcal{C} = \mathcal{C}^\top$ is semi-positive with respect to the displacement fields $\vec{w}_i$, $\vec{w}_j$, since the integration only affects the contact surface and is not influenced by the displacement fields within the bodies.

The sliding friction stress vectors on the contacting bodies read $\vec{t}_F^{(\alpha)} = \mu p \vec{e}_F^{(\alpha)}$ ($\alpha = i, j$), where $\vec{t}_F^{(j)} = -\vec{t}_F^{(i)}$. Thus, the virtual work of the sliding friction between i-j reads $\delta W_C^{(ij)} = \int_{\Gamma_C^{(ij)}} \delta(\vec{r}_j - \vec{r}_i) \cdot \left[-\vec{t}_F^{(i)} \right] da = \int_{\Gamma_C^{(ij)}} \delta\vec{g} \cdot \left[-\vec{e}_F^{(i)} \mu p(g_N) \right] da$, from which Taylor expansion yields

$$\Delta\left\{\delta W_C^{(ij)}\right\} = -\int_{\Gamma_C^{(ij)}} \delta\vec{g} \cdot \left[\mu_0 p_0 \Delta\vec{e}_F^{(i)} + \vec{e}_{F0}^{(i)} \mu_0 \Delta p \right] da, \tag{6}$$

where it has been assumed that the coefficient of sliding friction is constant. With $v_{rel,0}^{(ij)} = ||\mathbf{v}_{Tj}^\top \frac{\partial}{\partial\mathbf{x}}\vec{r}_{0j} - \mathbf{v}_{Ti}^\top \frac{\partial}{\partial\mathbf{x}}\vec{r}_{0i}||$ being the relative velocity in the linearization point, Taylor expansion of $\vec{e}_F^{(i)}$ and ommission of higher order terms yields

$$\Delta\vec{e}_F^{(i)} \approx \frac{1}{v_{rel,0}^{(ij)}} \Delta\vec{v}_{rel} = \frac{1}{v_{rel,0}^{(ij)}} \left[\Delta\dot{\vec{g}} + \mathbf{v}_{Tj}^\top \frac{\partial}{\partial\mathbf{x}}\vec{w}_j - \mathbf{v}_{Ti}^\top \frac{\partial}{\partial\mathbf{x}}\vec{w}_i \right]. \tag{7}$$
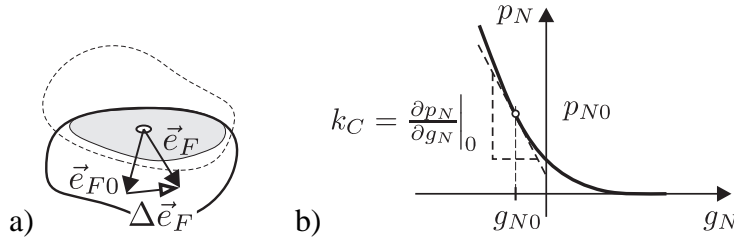
Figure 3: a) Linearization of the direction vector $\vec{e}_F$ of the friction within the contact between two bodies. b) Example of a constitutive contact law relating contact pressure p_N and distance g_N. Linearization about a working point.

4

With $\Delta p = -k_C \Delta g_N = -k_C \left(\vec{e}_N \cdot \Delta \vec{g} \right)$ one finally obtains

$$
\begin{aligned}
\Delta\{-\delta W_C\} \;=\; & \sum_{(ij)}^{n_C} \int_{\Gamma_C^{(ij)}} \delta\vec{g} \cdot \left\{ \left[\frac{\mu p_0}{v_{rel}^{(ij)}} \mathbb{I} \right]_0 \Delta\dot{\vec{g}} \right. \\
& \qquad + \left[\frac{\mu p_0}{v_{rel}^{(ij)}} \mathbb{I} \right]_0 \left(\mathbf{v}_{Tj}^\top \frac{\partial}{\partial \mathbf{x}} \vec{w}_j - \mathbf{v}_{Ti}^\top \frac{\partial}{\partial \mathbf{x}} \vec{w}_i \right) \\
& \qquad \left. - \left[\mu k_C \left(\vec{e}_F \otimes \vec{e}_N \right) \right]_0 \Delta\vec{g} \right\} \mathrm{d}a \\
=\; & \sum_{(ij)}^{n_C} \int_{\Gamma_C^{(ij)}} \delta\vec{g} \cdot \left\{ \mathcal{R}_1\!\left[\Delta\dot{\vec{g}}\right] + \mathcal{R}_2\!\left[\vec{w}_i, \vec{w}_j\right] + \mathcal{R}_3\!\left[\Delta\vec{g}\right] \right\} \mathrm{d}a, \qquad (8)
\end{aligned}
$$

where $\mathcal{R}_1 = \mathcal{R}_1^\top$ is a symmetric and positive semi-definite operator, while $\mathcal{R}_2 \neq \mathcal{R}_2^\top$, $\mathcal{R}_3 \neq \mathcal{R}_3^\top$ are nonsymmetric.

The physical interpretation of $\mathcal{C}$ as contact stiffness is obvious. The operators $\mathcal{R}_1$ and $\mathcal{R}_2$ stem from the changing direction of the friction stresses, while $\mathcal{R}_3$ arises from the change of contact pressure as the bodies deform.

For small values of $v_{rel,0}^{(ij)} \ll 0$ the operator $\mathcal{R}_1$ will become very large. However, the limit $v_{rel,0}^{(ij)} = 0$ is not valid since it would involve stiction, which was precluded. For the second operator $\mathcal{R}_2$ this may not be observed: since nominator and denominator are of the order of magnitude of the velocity parameters, it will not become singular. In general it is found that $\mathcal{R}_2$ has rather small influence on the system.

The operator $\mathcal{R}_3$ expresses the non-conservative influence of positional forces on the system and will be the reason of the flutter type instability. Please note, that this contribution is mainly controlled by the contact stiffness k_C, which will be investigated below.

2.3 Finite dimensional system dynamics

Eventually, discretization of equation (1) in conjuction with (8) leads to a system of ordinary differential equations of the form

$$
\mathbf{M}\ddot{\mathbf{q}} + \left(\mathbf{G} + \mathbf{D}_S + \mathbf{D}_F \right) \dot{\mathbf{q}} + \left(\mathbf{K} + \mathbf{K}^* + \mathbf{C} + \mathbf{R}_2 + \mathbf{R}_3 \right) \mathbf{q} = \mathbf{0} \qquad (9)
$$

where

$$
\begin{aligned}
\mathbf{M}\,,\ \mathbf{D}_S\,,\ \mathbf{K} \qquad & \text{are symmetric and positive definite,} & (10) \\
\mathbf{D}_F\,,\ \mathbf{C}\,,\ \mathbf{K}^* \qquad & \text{are symmetric and positive semi-definite,} & (11) \\
\mathbf{G} \qquad & \text{is skew-symmetric and} & (12) \\
\mathbf{R_2}\,,\ \mathbf{R_3} \qquad & \text{are non-symmetric.} & (13)
\end{aligned}
$$

Here the symbol $\mathbf{D}_F$ for the discretization of $\mathcal{R}_1$ has been chosen in order to stress the symmetry of $\mathbf{D}_F$. Hence, this problem belongs to the class of general gyroscopic-circulatory stability problems and thus may exhibit a complicated stability behaviour, including divergence and flutter ([2], [9] for instance).

The findings are summarized in table 1.

operator	stems from	affects system's	contributes Matrix
$\mathcal{R}_1$	changing friction direction	damping	$\mathbf{D}_F = \mathbf{D}_F^\top \geq 0$
$\mathcal{R}_2$	changing friction direction	stiffness	$\mathbf{R}_2 \neq \mathbf{R}_2^\top$
$\mathcal{R}_2$	fluctuation of contact pressure	stiffness	$\mathbf{R}_3 \neq \mathbf{R}_3^\top$

Table 1: Overview on linearized frictional contributions to the perturbation equations.

3 CONSTITUTIVE CONTACT LAW

As has been found, the contact stiffness k_C is one of the influencing parameters to the frictional contributions $\mathcal{R}_3$ which is the cause of the flutter instability – thus, it is necessary to give it a physical meaning. To this end, a constitutive contact law following the basic idea of Greenwood-Williamson is adopted [4], [10].

Assume two rough surfaces z_1, z_2, where the heights of the asperities of each obey Gaussian distribution functions with standard deviations σ_1 and σ_2. Thus, the distance $z = z_2 - z_1$ itself is also a gaussian stochastic process with distribution density $\Phi(z)$, whose standard deviation is given by

$$\sigma = \sqrt{\sigma_1^2 + \sigma_2^2}. \tag{14}$$

With this, the normalized vertical coordinate $s = z/\sigma$ along $\vec{e}_N$ and the normalized distance $h = g_N/\sigma$ are introduced. The gap function g_N is interpreted as the distance of the nominal surfaces located at the mean values $\bar{z}_{1/2}$ (cf. fig. 4 a). The asperities of both surfaces are locally approximated by spherical caps with the radii of curvature κ_1 and κ_2, which are made of materials with the Young's-moduli E_1 and E_2. If Hertzian contact theory is applied to the local behaviour of the asperities, the effective values

$$\frac{1}{\kappa} = \frac{1}{\kappa_1} + \frac{1}{\kappa_2} \quad \text{and} \quad \frac{1}{E} = \frac{1 - \nu_1^2}{E_1} + \frac{1 - \nu_2^2}{E_2} \tag{15}$$

may be assigned to the resulting process z, which describes the distance of the asperities.
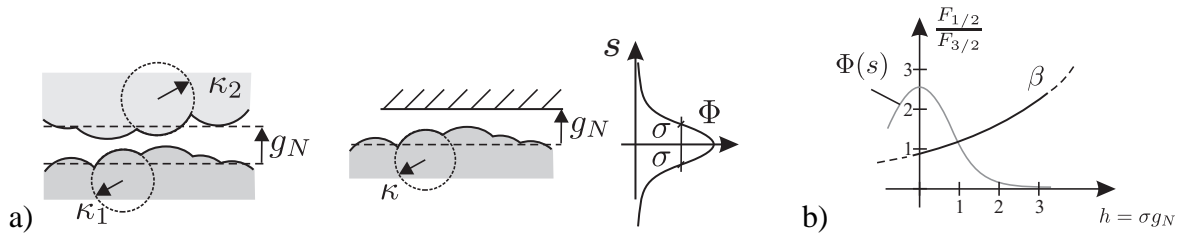
Figure 4: Rough surfaces: a) Geometry, kinematics and distribution density of the asperity heights. b) Distribution density and $\beta = F_{3/2}/F_{1/2}$.

The compression of an asperity of height s reads $d = s - h$. Thus, applying Hertzian contact theory to the spherical caps yields the contact pressure

$$p = \frac{P}{A} = \frac{4}{3}\eta E \sqrt{\kappa \sigma^3} F_{3/2}(h), \tag{16}$$

where η is the number of asperities per unit area and $F_n(h) = \int_h^\infty (s - h)^n \Phi(s) \mathrm{d}s$ is a special moment function of the distribution density Φ. The density η is difficult to measure and thus is

unknown in most practical applications. In order to circumvent this problem, one may formulate

$$\frac{1}{p}\frac{\mathrm{d}p}{\mathrm{d}g_N}\Big|_{p=p_0} = \frac{3}{2\sigma}\frac{F_{1/2}(h)}{F_{3/2}(h)}\Big|_{h=h(p_0)} = \frac{3}{2\sigma}\beta(h_0) \tag{17}$$

to describe the contact pressure in the vicinity of a working point (h_0, p_0). Since β only weakly depends on h, for many applications it may be assumed that $\beta \approx$ const around the working point. This latter relation can readily be integrated to

$$p(g_N) = p_0 \exp\left(\frac{3\beta}{2\sigma}(\Delta g_N)\right). \tag{18}$$

Hence, the parameters of exponential constitutive contact laws (like in ABAQUS, [5]) may easily be related to toplogical properties of the surface, provided β may be reasonably estimated, as is the case for many applications. It shall be mentioned that similar results may be derived by using exponential approximations of Φ without the need to assume Hertzian contact ([4] for instance). However, such approaches involve the quite uncertain parameter η, which has been eliminated by the approach stated above.

Taylor expansion yields $p(g_{N0} + \Delta g_N) \approx p_0 + k_C \Delta g_N$ where

$$k_C = p_0 \frac{3\beta}{2\sigma}. \tag{19}$$

It is noted, that the linearized contact stiffness depends on the standard deviation σ of the height distribution as well as on the contact pressure p_0 in the linearization point.

Please note that the presented approach relies on Hertzian contact theory, thus assuming linear elastic behaviour. In order to test the applicability for problematic cases, the plasticity index Ψ could be used for instance (e.g. [4]).

4 EXAMPLE: rotating Euler-Bernoulli annulus sliding through Winkler-type bedding

Above results are exemplified with the example of a rotating Euler-Bernoulli-ring in frictional guides, cf. fig. 5 a), which may be interpreted as a simple model for a vehicle disc brake. The example comprises an annular Euler-Bernoulli beam (body 2: radius R, height h, width
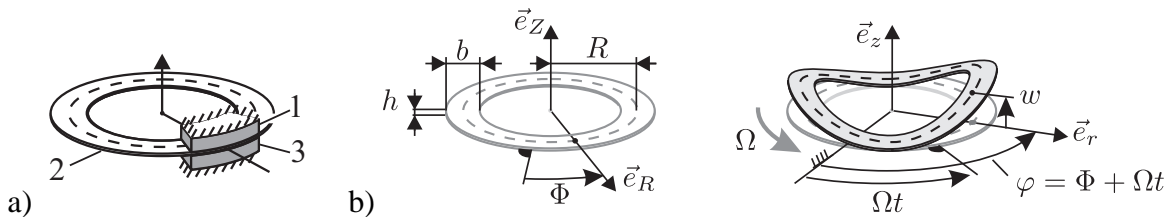
Figure 5: Example problem: rotating Euler-Bernoulli ring: a) System of bodies. b) Kinematics of the ring: material reference frame (left) and spatial frame (right).

b, density ϱ, bending stiffness EI) which rotates with the angular velocity Ω about the vertical axis. The annulus slides through two frictional pads (friction coefficient μ =const), that are modelled as Winkler foundations (bodies 1 and 3, height h_p, width b, density ϱ_p, foundation stiffness k, spatial extent $-\varphi_0 \le x \le \varphi_0$).

In a reference configuration, the material coordinate Φ is introduced, while the spatial coordinate φ describes the position after the rigid body motion. The rigid body transport motion relates the spatial frame to the reference frame via $\varphi = \Phi + \Omega t$.

The displacement of the beam's neutral fibre is denoted by $w(\varphi, t)$, while $w_1(\varphi, t)$ and $w_3(\varphi, t)$ refer to the displacements of the upper and lower friction pads' surfaces. Furthermore, the superscripts $()^+$ and $()^-$ to $w(\varphi, t)$ refer to the upper and lower surface of the beam. Thus, surface points on the friction pads have the position vectors

$$\vec{r}_1(r, \varphi, z) = r\vec{e}_r + (w_{10} + w_1)\vec{e}_z = (r, 0, w_{10})_{r\varphi z}^\top + (0, 0, w_1)_{r\varphi z}^\top = \vec{r}_{T1} + \vec{w}_1 \tag{20}$$

$$\vec{r}_3(r, \varphi, z) = r\vec{e}_r + (w_{30} + w_3)\vec{e}_z = (r, 0, w_{30})_{r\varphi z}^\top + (0, 0, w_3)_{r\varphi z}^\top = \vec{r}_{T3} + \vec{w}_3. \tag{21}$$

Here, the brackets $(\dots)_{r\varphi z}$ contain the coefficients to the unit vectors but not the coordinates.

The position vectors of points of the neutral fibre as well as on the beam's surfaces read

$$\vec{r}_2(r, \varphi, z) = (r, 0, 0)_{r\varphi z}^\top + (0, 0, w)_{r\varphi z}^\top = \vec{r}_{T2} + \vec{w}_2 \tag{22}$$

$$\vec{r}_2^+(r, \varphi, z) = (r, 0, h/2)_{r\varphi z}^\top + (0, -h/(2R)\, w', w)_{r\varphi z}^\top = \vec{r}_{T2}^+ + \vec{w}_2^+ \tag{23}$$

$$\vec{r}_2^-(r, \varphi, z) = (r, 0, -h/2)_{r\varphi z}^\top + (0, +h/(2R)\, w', w)_{r\varphi z}^\top = \vec{r}_{T2}^- + \vec{w}_2^- \tag{24}$$

(cf. fig. 2 b). Please note that in order to formulate the displacement of the beam's surface points Euler's normal hypothetis has been used. The displacement fields within the friction pads are assumed to vary linearly with z, i.e.

$$w_{p1}(z) = w_1 \left(1 - \frac{(z - w_{10})}{h}\right) \quad , z = w_{10} \dots (w_{10} + h_p) \tag{25}$$

$$w_{p3}(z) = w_3 \left(\frac{z - w_{30}}{h}\right) \quad , z = w_{30} \dots (w_{30} + h_p). \tag{26}$$

Eventually, the dynamics of the system is described by

$$\int_0^{2\pi} \delta w \left(\varrho bh(\ddot{w} + 2\Omega\dot{w}' + \Omega^2 w'') + EIw''''\right) d\varphi \tag{27}$$

$$+ \sum_{i=1,3} \int_{-\varphi_0}^{\varphi_0} \delta w_i \left(\frac{\varrho_p bh_p}{3}\ddot{w}_i + kw_i\right) d\varphi \quad + \Delta\{\delta\Pi_C - \delta W_C\} = 0. \tag{28}$$

The contact contributions $\Delta\{\delta\Pi_C - \delta W_C\}$ between the sliding beam (body 2) and the upper and lower pad (body 1, 2 resp.) are derived using the theory stated above. In order to obtain equations of similar structure for both contacts, it is advantageous to calculate $\Delta W_C = \Delta W_C^{(12)} + \Delta W_C^{(32)}$. The necessary tangential systems read

$$\text{body 1:} \quad \vec{e}_F^{(1)} = (0, 1, 0)_{r\varphi z}^\top \quad , \qquad \vec{e}_N^{(1)} = (0, 0, -1)_{r\varphi z}^\top \tag{29}$$

$$\text{body 3:} \quad \vec{e}_F^{(3)} = (0, 1, 0)_{r\varphi z}^\top \quad , \qquad \vec{e}_N^{(3)} = (0, 0, +1)_{xy}^\top. \tag{30}$$
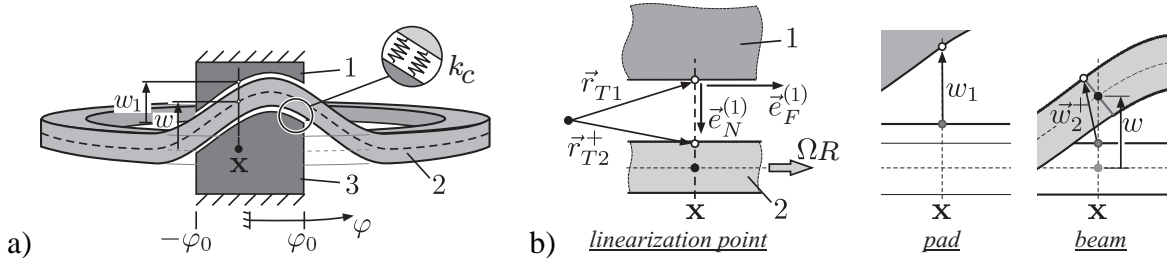
Figure 6: Kinematics of the system in the contact: a) Contact zone $\varphi = -\varphi_0 \dots \varphi_0$, displacement fields w of the neutral fibre and w_1, w_2 of the friction pads' surfaces. b) Contact between body 1 (upper friction lining) and body 2 (ring): configuration in the linearization point with local tangential frame (left), displacement fields about the linearization point.

The linearized gap vectors read

$$\Delta \vec{g}^{(12)} = \vec{w}_2^+ - \vec{w}_1 = (0, -h/(2R)\, w', w - w_1)_{r\varphi z}^\top \tag{31}$$

$$\Delta \vec{g}^{(32)} = \vec{w}_2^- - \vec{w}_3 = (0, +h/(2R)\, w', w - w_3)_{r\varphi z}^\top \tag{32}$$

and thus the corresponding variations read $\delta \vec{g}^{(12)} = \delta(\Delta \vec{g}^{(12)}) = (0, -h/(2R)\, \delta w', \delta w - \delta w_1)_{r\varphi z}^\top$ and $\delta \vec{g}^{(32)} = \delta(\Delta \vec{g}^{(32)}) = (0, +h/(2R)\, \delta w', \delta w - \delta w_3)_{r\varphi z}^\top$.

Hence, inserting these quantities into (5) the normal contact contributions of the upper contact for instance yields

$$\Delta \left\{ \delta \Pi_C^{(12)} \right\} = \int_{-\varphi_0}^{\varphi_0} b k_C \begin{bmatrix} 0 \\ -h/(2R)\, \delta w' \\ \delta w - \delta w_1 \end{bmatrix}^\top \left[\begin{pmatrix} 0 \\ 0 \\ -1 \end{pmatrix} \otimes \begin{pmatrix} 0 \\ 0 \\ -1 \end{pmatrix} \right] \begin{bmatrix} 0 \\ -h/(2R)\, w' \\ w - w_1 \end{bmatrix} \mathrm{d}\varphi \tag{33}$$

$$= \int_{-\varphi_0}^{\varphi_0} b k_C \, (\delta w_1 - \delta w)\, (w_1 - w)\, \mathrm{d}\varphi \tag{34}$$

and from equation (8) one gets the virtual work of the tangential forces

$$\Delta \left\{ \delta W_C^{(12)} \right\} = \int_{-\varphi_0}^{\varphi_0} \begin{bmatrix} 0 \\ -h/(2R)\, \delta w' \\ \delta w - \delta w_1 \end{bmatrix}^\top \left\{ \left[\frac{\mu p_0}{\Omega} \mathbf{I} \right] \begin{bmatrix} 0 \\ -h/(2R)\, \dot{w}' \\ \dot{w} - \dot{w}_1 \end{bmatrix} \right. \tag{35}$$

$$\left[\frac{\mu p_0}{\Omega} \mathbf{I} \right] \Omega \frac{\partial}{\partial x} \begin{bmatrix} 0 \\ -h/(2R)\, w' \\ w \end{bmatrix} \tag{36}$$

$$\left. -\mu k_C \left[\begin{pmatrix} 0 \\ 1 \\ 0 \end{pmatrix} \otimes \begin{pmatrix} 0 \\ 0 \\ -1 \end{pmatrix} \right] \begin{bmatrix} 0 \\ -h/(2R)\, w' \\ w - w_1 \end{bmatrix} \right\} b\, \mathrm{d}\varphi$$

$$= \int_{-\varphi_0}^{\varphi_0} \delta w' \frac{h^2}{4R^2} \left[\frac{\mu p_0}{\Omega} \right] \dot{w}' + \delta[w - w_1] \frac{\mu p_0}{\Omega} [\dot{w} - \dot{w}_1]\, b\, \mathrm{d}\varphi \tag{37}$$

$$+ \int_{-\varphi_0}^{\varphi_0} \delta w' \frac{h^2}{4R^2} [\mu p_0]\, w'' + \delta[w - w_1]\mu p_0 w'\, b\, \mathrm{d}\varphi \tag{38}$$

$$- \int_{-\varphi_0}^{\varphi_0} \delta w' \frac{h}{2R} \mu k_C [w - w_1]\mu p_0 w'\, b\, \mathrm{d}\varphi. \tag{39}$$

The terms $\Delta \left\{ \delta \Pi_C^{(32)} \right\}$, $\Delta \left\{ \delta W_C^{(32)} \right\}$ arising from the second contact on the lower surface are derived analogously and are of similar structure. At this point, the symmetry properties of the frictional terms turn obvious: while equation (37) will contribute symmetric terms to the system's damping, the remaining (38) and (39) are non-symmetric positional contributions.

In order to allow for further interpretation the frictional terms the linearized upper friction traction $\Delta \vec{t}^+$ may be decomposed according to $\Delta \vec{t}^+ = \mu p_0 \Delta \vec{e}_F + \vec{e}_{F0} \mu \Delta p + \vec{e}_{F0} p_0 \Delta \mu =$

$\Delta t_\varphi \vec{e}_\varphi + \Delta t_z \vec{e}_z$. Thus, rearrangement of (37)-(39) yields

$$\Delta\left\{\delta W_C^{(12)}\right\} = \int_{-\varphi_0}^{\varphi_0} \delta w' \frac{h}{2R}\Delta t_\varphi + \delta[w - w_1]\Delta t_z\, b\mathrm{d}\varphi \tag{40}$$

$$= \int_{-\varphi_0}^{\varphi_0}\left\{\delta w' \frac{h}{2R}\left[\mu p_0\Big(\underbrace{\frac{h}{2\Omega R}\dot{w}' + \frac{h}{2R}w''}_{\Delta\vec{e}_F\cdot\vec{e}_\varphi}\Big) - \mu\underbrace{k_C(w - w_1)}_{\Delta p}\right]\right. \tag{41}$$

$$\left. + (\delta w - \delta w_1)\mu p_0\left[\underbrace{\frac{1}{\Omega}(\dot{w} - \dot{w}_1) - w'}_{\Delta\vec{e}_F\cdot\vec{e}_z}\right]\right\}b\mathrm{d}\varphi. \tag{42}$$

The first addend in (40) is readily found to express the virtual work of the torque $h/2\,\Delta t_\varphi$, while the second is the virtual work of the vertical component Δt_z (cf. fig. 7). Moreover, the first and the last underbraced term in (41), (42) are components of $\Delta\vec{e}_F$, consisting of the local derivative together with the corresponding convective parts.
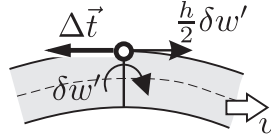
Figure 7: Physical interpretation of the contributions entering the virtual work of the friction: the traction $\Delta\vec{t}$ does virtual work along the virtual displacement $\frac{h}{2}\delta w'$.

Finally, in order to discretize the weak formulation (28) the spatial fields may be approximated by a Ritz-type ansatz of the form $w_k = \sum_{i=1}^K f_{ki}(\varphi)q_{ki}(t) = \mathbf{\Phi}_k\mathbf{q}_k$ of order K, where the matrices $\mathbf{\Phi}_k(\mathbf{x})$ contain spatial ansatz functions. The virtual displacements read $\delta w_k = \delta\mathbf{q}_k^\top\mathbf{\Phi}_k^\top$. Although the continuum is moving, the spatially fixed friction pads suggest spatially fixed vibration patterns; this assumption is validated by experimental observations. Thus, the harmonic eigenfunctions of the non-rotating beam are chosen as ansatz functions, hence

$$w_k = [\ldots\cos n\varphi \ \sin n\varphi\ldots]\begin{bmatrix}\vdots\\q_{k\ 2n-1}\\q_{k\ 2n}\\\vdots\end{bmatrix} = \mathbf{\Phi}_k\mathbf{q}_k \quad,\qquad k,n = 1,\ldots,K. \tag{43}$$

In general, the contact pressure $p_0 = p_0(\varphi)$ in the steady state will be spatially distributed over the contact zone. Hence, if a constitutive contact law like (48) is used, the contact stiffness $k_C = k_C(p_0(\varphi))$ will also depend on the position. For this case, the perturbation equations of the steady state get

$$\mathbf{M}\ddot{\mathbf{q}} + \Omega\mathbf{G}\dot{\mathbf{q}} + \frac{\mu}{\Omega}\mathbf{D}_F(p_0)\dot{\mathbf{q}} + \left[\mathbf{K} + \Omega^2\mathbf{K}^* + \mathbf{K}_N(k_C) + \mu\mathbf{R}_3(k_C) + \mu\mathbf{R}_2(p_0)\right]\mathbf{q} = \mathbf{0} \tag{44}$$

$$p_0 = p_0(\varphi) \quad,\qquad k_C = k_C(p_0). \tag{45}$$

The frictional influence on the system produces the matrix $\mathbf{D}_F$, $\mathbf{R}_2$ and $\mathbf{R}_3$ which stem from $\mathcal{R}_1$, $\mathcal{R}_2$ and $\mathcal{R}_3$ respectively (cf. eq. (8)). The coefficient of friction has been assumed constant over the contact.

Since an analytical principle has been used and the linearization point is a stable static equilibrium, $\mathbf{M} = \mathbf{M}^\top$ and $\mathbf{K} = \mathbf{K}^\top$ are symmetric and positive definite. The gyroscopic terms $\mathbf{G} = -\mathbf{G}^\top$ are skew-symmetric. Moreover, as predicted above $\mathbf{D}_F = \mathbf{D}_F^\top$, $\mathbf{K}_N = \mathbf{K}_N^\top$ are symmetric and positive semi-definite and $\mathbf{R}_2$ and $\mathbf{R}_3$ are not symmetric. Usually, the entries of $\mathbf{R}_3$ are found to be much larger than those of $\mathbf{R}_2$. Equation (44) is a gyroscopic-circulatory system, which may exhibit flutter instability due to the non-symmetric positional forces (e.g. [2], [9], [1]).

4.1 Steady-state stability

It is assumed, that the trivial solution of (44) belongs to stable static solution and that Ω and thus the centrifugal terms $\Omega^2 \mathbf{K}^*$ are comparatively small. Moreover, in most cases curvature w'' and the inclination w' are small and thus the influence of $\mathbf{R}_2$ is indeed found to be negligible. Thus, equation (44) simplifies to

$$\mathbf{M}\ddot{\mathbf{q}} + \Omega\mathbf{G}\dot{\mathbf{q}} + \frac{\mu}{\Omega}\mathbf{D}_F(p_0)\dot{\mathbf{q}} + \left[\mathbf{K} + \mathbf{K}_N(k_C) + \mu\mathbf{R}_3(k_C)+\right]\mathbf{q} = \mathbf{0} \qquad (46)$$

$$p_0 = p_0(\varphi) \quad , \qquad k_C = k_C(p_0). \qquad (47)$$

Here, the trivial solution may only get unstable due to the non-symmetric, non-conservative contributions $\mathbf{R}_3$, which may lead to a flutter-type instability. Although this is the actual reason leading to instability, it may be strongly affected by velocity dependent terms stemming from dissipation and transport motion.

Furthermore, since all frictional contributions depend on the contact parameters p_0 and k_C, they will have a significant effect as well. The contact stiffness is chosen according to equation (19). For instance, for typical working conditions in vehicle brakes β may be estimated as $\beta \in [4/3 \dots 6/3]$. Moreover, it is found by experiments that the distribution of the asperities may be adequately described by Gaussian distributions. Typical standard deviations found are $\sigma_{new} \approx 20\mu$ for new brake pads and $\sigma_{worn} \approx 5\mu$m for worn pads [10]. Thus, choosing an average value of β yields

$$k_C \approx p_0 \frac{5}{2\sigma}, \qquad (48)$$

where $p_0 = p_0(\varphi)$ and thus k_C may vary within the contact zone.

4.1.1 Basic mechanism of flutter instability

Due to the assumptions $\mathbf{D} \geq 0$ and $(\mathbf{K} + \mathbf{K_N}) > \mathbf{0}$ together with $\mathbf{M} > 0$, divergence instability is ruled out and thus the trivial solution may only get unstable due to flutter, which is produced by the non-symmetric contributions to the positional forces.

In this context, it is emphasized that the Theorem of Thomson and Tait does not apply due to the non-symmetric stiffness matrix and thus, it is not assured that adding dissipation or gyroscopic terms may not destabilize the trivial solution (e.g. [12] , [9], [6], [1]). Hence, investigating the simplified MKN-system in order to obtain an estimate of the stability border is not a valid approach – moreover, the influence of velocity-proportional contributions may alter the stability border significantly, as will be demonstrated below. However, the underlying mechanism leading to instability is flutter.

Circulatory system Although an investigation of the simplified MKN-system will not yield a reliable estimate of the stability border of the full system, in a first approach the undamped, non-gyroscopic circulatory system

$$\mathbf{M\ddot{q}} + [\mathbf{K} + \mathbf{K}_N(k_C) + \mu\mathbf{R}_3(k_C)+]\,\mathbf{q} = \mathbf{0} \tag{49}$$

will be used to demonstrate the basic mechanism of flutter. From equation (49), it is obvious
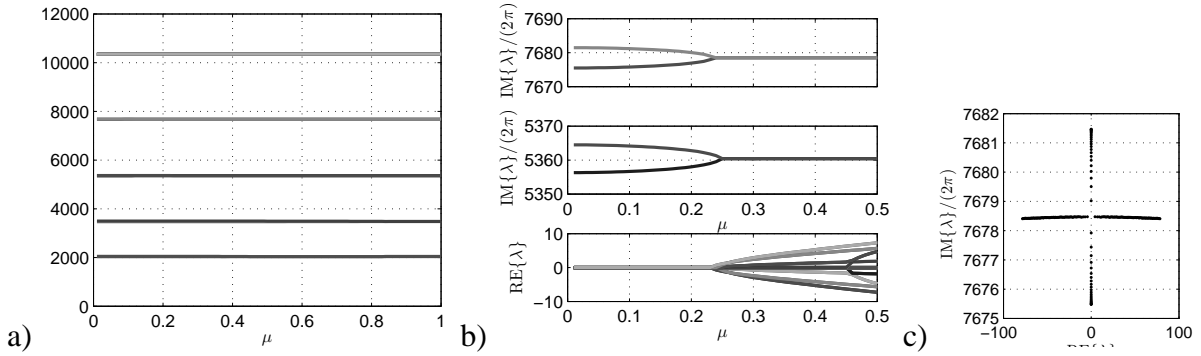
Figure 8: Eigenvalues of a circulatory system (MKN): a) Imaginary parts of the eigenvalues as the load parameter μ is changed. Divergence does not occur since no imaginary part vanishes. b) Imaginary parts of the first two eigenvalues that become unstable and corresponding real parts (lower subfigure) as functions of μ. c) Eigenpaths of the first unstable eigenvalue in the complex plane.

that the influence of the non-symmetric frictional influence $\mathbf{R}_3$ is controlled by the parameter μ, which is sometimes referred to as load parameter. From equation (39) it is clear that the frictional contributions also depend on the contact stiffness as well as on the spatial extent of the contact zone φ_0. Please note, that the contact stiffness k_C and the coefficient of friction μ appear as product and thus will influence the result equally. The rotational speed Ω does not influence the behaviour of the simplified equation (49).

In order to examine the stability of the trivial solution, the ansatz $\mathbf{q} = \mathbf{r}\mathrm{e}^{\lambda t}$ is used to derive from (49) the corresponding polynomial eigenvalue problem for the eigenvalues λ.

Figure 8 displays the behaviour of the eigenvalues of (49) in dependence of μ: subfigure a) displays the imaginary parts of the eigenvalues and proves that divergence does not appear since no eigenfrequency vanishes. Part b) shows the real parts (bottom) and the imaginary parts (eigenfrequencies) of the first two eigenvalues that become unstable. Subfigure c) shows the behaviour of the first unstable eigenvalue in the complex plane. The shown eigenvalue behaviour is the typical scenario for flutter instability: as the load parameter μ – i.e. the parameter that controls the influence of the non-symmetric influences on the system – is varied, pairs of eigenvalues mutually approach (8 b). Initially being pureley imaginary, they converge and after merging at a distinct $\mu = \mu_{crit}$, they leave the imaginary axis into opposite halfplanes of the complex plane (8 c), causing instability.

The non-conservative part $\mathbf{R}_3$ depends on the contact stiffness k_C as well as on the integration limits $\varphi_0 = \arctan\frac{L_p}{R}$. Figure 9 shows the stability border for varying contact stiffness for two different pad lengths L_p. The strong effect of k_C emphasizes the need of either experimentally verified values or physically sensible constitutive contact models, relating measurable surface properties to contact stiffness values. Furthermore, it can be seen that also the spatial extent of the contact (described by L_p) has a strong effect.
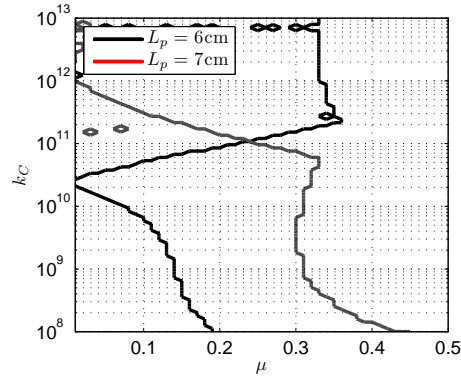
Figure 9: Stability borders of the circulatory system (MKN) for varying coefficient of friction μ and contact stiffness k_C, outlined for two different lengths L_p of the contact zone. Note the significant impact of the contact stiffness on stability.

Full gyroscopic-circulatory system As mentioned before, it is not possible to use the simplified undamped non-gyroscopic problem to examine the stability. Thus, it is necessary to investigate the full system. As a well known fact, velocity-proportional contributions to circula-
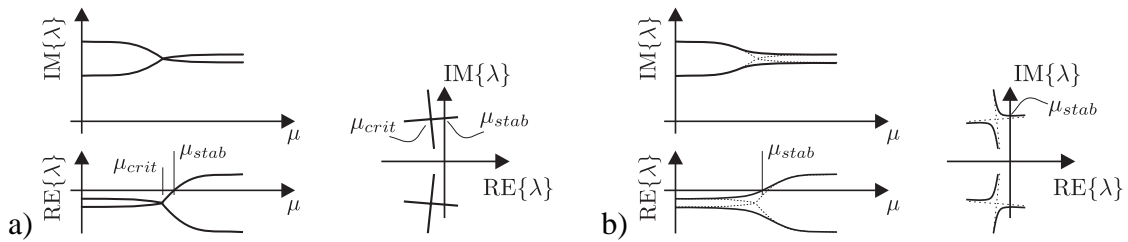
Figure 10: Schematic of the eigenvalue behaviour of general systems with dissipation, gyroscopic effects and circulatory contributions (MDGKN): a) Special case of "modal" velocity proportional contributions, i.e. that eigenvectors of the pure circulatory system (MKN) are also eigenvectors of the full system (MDGKN). b) General case.

tory systems may alter the stability border drastically. In particular it is found that the transition scenario of the eigenvalues for changing load parameter μ is totally different to that of the purely circulatory system. Here again, pairs of eigenvalues still approach and two genuine scenarios may be distinguished:
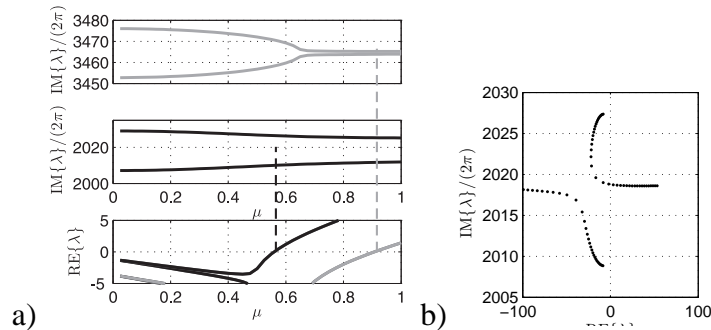
Figure 11: Eigenvalues as function of μ for a small angular velocity ($\Omega = 0.5\pi/s$): a) Imaginary parts of the first two unstable eigenvalues and corresponding real parts. b) Eigenpath in the complex plane.

13
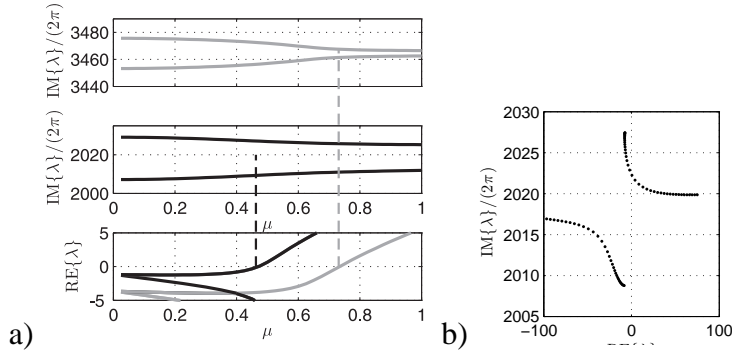
Figure 12: Eigenvalues as function of μ for a higher angular velocity ($\Omega = \pi/s$): a) Imaginary parts of the first two unstable eigenvalues and corresponding real parts. b) Eigenpath in the complex plane.
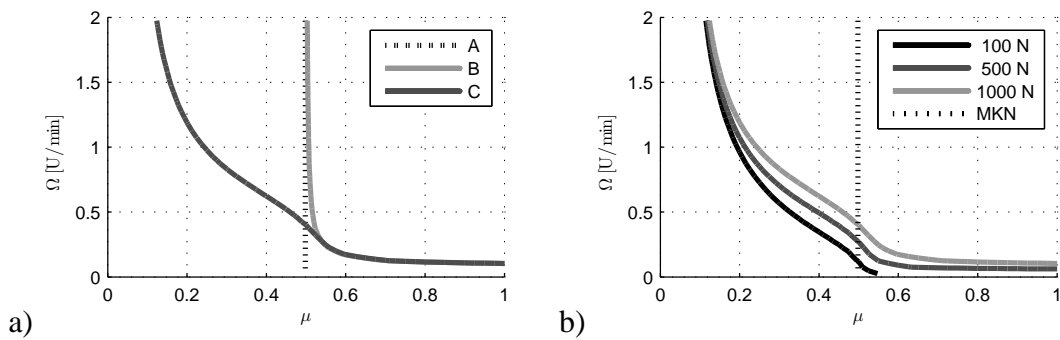
Figure 13: Stability border: a) Influence of different modelling levels on the stability. (A) - damped circulatory system (MDKN), (B) circulatory system with frictional damping (MDKN), (C) full system (MDGKN). Obviously the gyroscopic contributions may have a strong effect even at low speeds. b) Influence of the normal force F_N on the friction linings for a constant contact stiffness (c_N =const).

a) If the velocity proportional terms fulfill the conditions of modal "damping" – i.e. if $\mathbf{P} = (\mathbf{D} + \mathbf{G})$ and $\mathbf{Q} = (\mathbf{K} + \mathbf{N})$ are interchangeable in the sense of $(\mathbf{M}^{-1}\mathbf{Q})(\mathbf{M}^{-1}\mathbf{P}) = (\mathbf{M}^{-1}\mathbf{P})(\mathbf{M}^{-1}\mathbf{Q})$ – the transition scenario of the eigenvalues involves a critical point where two imaginary parts merge. However, this critical point will in general not mark the stability border. This case is outlined in figure 10 a). This constellation may only occur in very special situations, since the componentes of $\mathbf{P}$ and $\mathbf{Q}$ stem from different independent physical effects – friction, motion of the continuum, etc. – which change as the corresponding parameters are varied. Thus, this case will only very unlikely occur.

b) In general, the velocity proportional terms will not be "modal" in the sense of interchangeble matrices $(\mathbf{M}^{-1}\mathbf{P})$ and $(\mathbf{M}^{-1}\mathbf{Q})$. Then also, two eigenvalues will mutually approach – however, they will not merge. Thus, there will be no distinguished critical point and the stability border may not be detected by only looking at the imaginary part. This scenario is outlined in figure 10 b). This is the general scenario and will almost always be the case.

Figures 11 and 12 show the corresponding results for the discussed example problem: subfigures a) show imaginary and real parts of the first two eigenvalues that become unstable, while subfigures b) display the eigenpaths in the complex plane. It is obvious that the influence of the non-modal velocity proportional contributions leads to a behaviour of the eigenvalues which is more complex than that of the purely circulatory system.

The influence of the gyroscopic term $\mathbf{G}$ – stemming from the transport motion Ω – is shown in figure 13 a), which displays the stability border of the example system for different modelling levels. The dotted line (A) denotes the stability border of the ciruclatory system (MDKN) with symmetric structural damping $\mathbf{D}_S$, but without frictional damping and gyroscopic effects. In a next step towards the full system, the gray line (B) outlines the stability border of the circulatory system (MDKN) with symmetric dissipation $\mathbf{D}_S + \mathbf{D}_F$, comprising structural damping as well as the damping $\mathbf{D}_S$ arising from the linearized friction forces. Finally, the black line (C) is the stability border of the full system (MDGKN), comprising all dissipative effects in $\mathbf{D}$ as well as the gyroscopic terms $\mathbf{G}$ due to the transport motion.

Figure 13 b) shows the influence of the normal force on the brake linings of the full system for constant contact stiffness $c_N = $const. As the normal force is increased, the pressure $p_0 = F_N/A$ increases and thus the influences of the frictional damping rises.

4.1.2 Influence of contact tribology and pressure distribution

The previous considerations did not account for the influence of parameters related to the tribological behaviour of the contact, namely the contact stiffness k_C and the pressure distribution $p_0 = p_0(\varphi)$ within the contact.

Assuming asperity heights obeying a Gaussian distribution, the contact stiffness may be expressed by equation (48), i.e. $k_C = p_0 \frac{5}{2\sigma}$. Thus, the contact stiffness depends linearly on the local contact pressure p_0 in the linearization point and further depends on the RMS of the distribution of the asperity heights.

Figure 14 displays the contact stiffness as function of σ of the asperity heights distribution and of the local contact pressure p_0 in the linearization point.
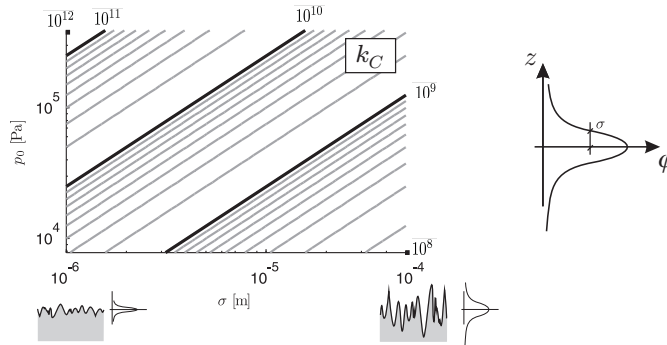
Figure 14: Contact stiffness k_C for different asperity height RMS σ and local pressure p_0.

In general, the local contact pressure will be spatially distributed, depending on the overall force applied to the friction linings as well as on the elastic behaviour of the structure. Thus, the contact stiffness as well will vary over the contact area. Figure 15 gives a survey on the influence of σ and $F = \int p \, \mathrm{d}a$ for two different contact pressure distributions

$$\text{I)} \qquad p = p_0 = \text{const} \qquad , \qquad p_0 = \frac{F_N}{A} \tag{50}$$

$$\text{II)} \qquad p = p_{max} \cos\left(\frac{\pi}{2} \frac{\varphi}{\varphi_0}\right) \qquad , \qquad p_{max} = \frac{\pi}{2} p_0. \tag{51}$$

As is clear to see, the topography parameter σ as well as the distribution of the contact pressure have a tremendous influence on the stability behaviour. In general, the $\cos$ −like pressure

15

distribution II) seems more squeal-proof than the constant pressure I), which might be due to the fact that only a smaller region es exerted to higher pressures. Concerning the influence of σ, no obvious rule is observable.

These results correspond to the experimental observations that squealing systems (like vehicle brakes) often start squealing after a certain period of usage, i.e. when σ has been changed by wear. Furthermore, it is known from practice that even small changes in the elastic structure or of the point of application of the lining force may change the overall acoustic behaviour.
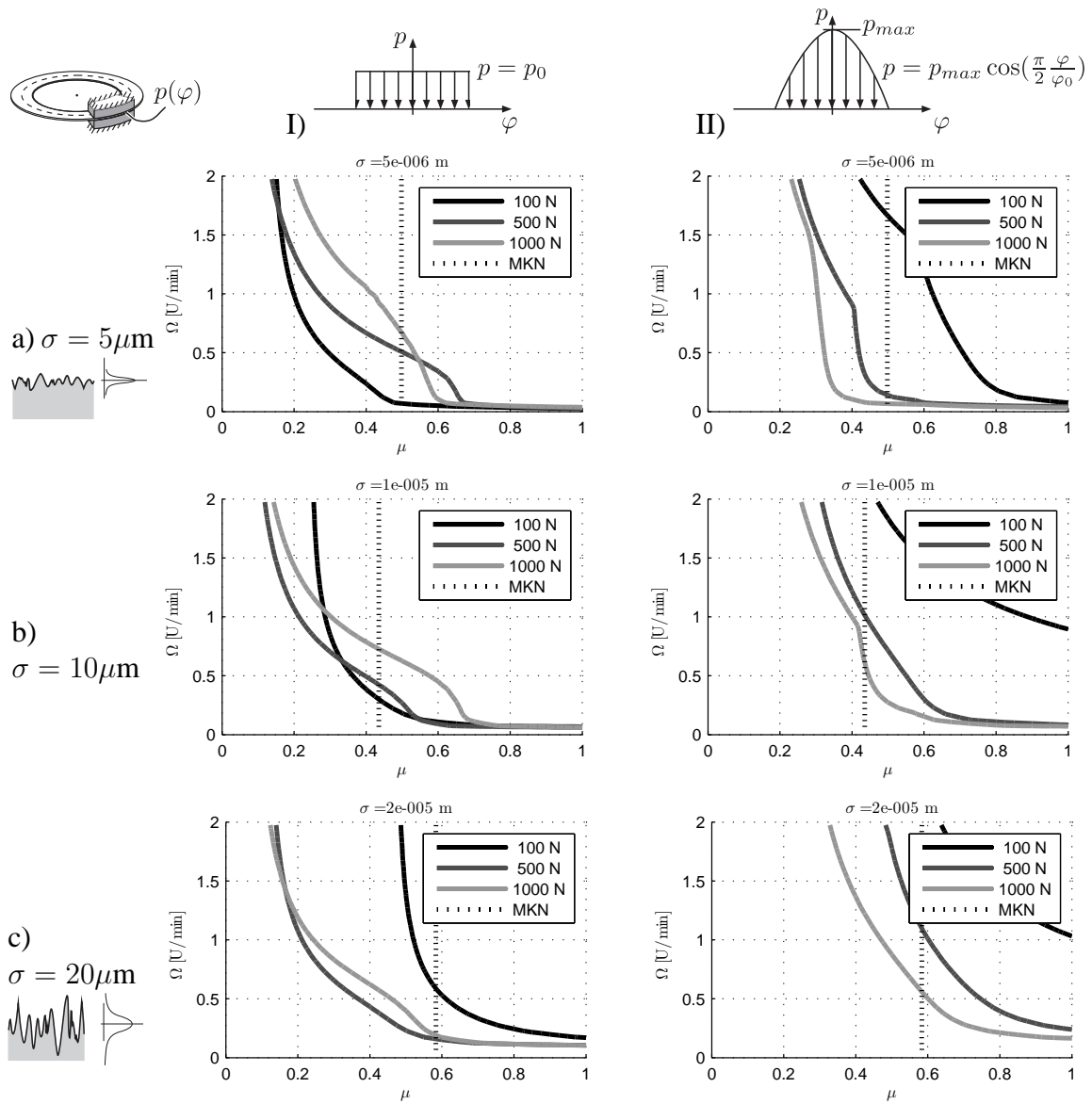
Figure 15: Stability charts as function of the surface topography and contact pressure distribution.

5   Conclusion

Using an abstract and thus general approach, the structure of the equations of motion of a system of moving bodies has been outlined. From this, the structure of the perturbation equations arising from linearization about a stationary solution has been stated, which comprises gyroscopic contributions due to the transport motion. Special attention has been set on the frictional contributions, namely on definiteness and symmetry of the corresponding differential operators. It is emphasized that these findings have been derived without relying on specific structural models (like beams, plates, ...) and thus are universally valid. The general findings about frictional influences to the perturbation equations are summarized in table 1.

Moreover, a simple constitutive contact model based on the theory of Greenwood-Williamson as well as on Hertzian contact theory is developed, which overcomes some difficulties in determining specific parameters needed in the classical G&W model. It is found that for many engineering problems the contact pressure is given by an exponential function, which depends on the RMS value of the asperity heights as parameter of the surface topography.

Finally, the findings are demonstrated using an example problem of a rotating Euler-Bernoulli ring, which slides through friction pads. which may be interpreted as simple model for the examination of brake squeal. In order to clarify further findings, basic results of the theory of general system with special emphasis on gyroscopic-circulatory systems are recapitulated.

It is demonstrated that the gyroscopic contributions due to the transport motion may have a significant effect on the stability border even for low speeds. Furthermore, it is found that the contact stiffness and thus the constitutive contact model is of major importance for stability assessments since it may alter the stability behaviour tremendously. The presented contact model relates the contact stiffness to surface topography and local contact pressure and it is found, that the spatial distribution of the contact pressure may also have a strong effect on the stability.

Appendix: Simulation parameters

Unless subjected to variations, the parameters used in the example problems (cf. fig. 5) are:

rotating ring

mean radius:	$R = 0.15$ m	width:	$b = 0.08$ m
thickness:	$h = 0.02$ m		
Y.-Modulus:	$E = 2.11 \cdot 10^{11}$ Pa	density:	$\rho = 7.8 \cdot 10^3$ kg/m^3

friction pads

thickness:	$h_p = 0.01$ m	length:	$L_p = 0.16$ m	width:	$b_p = b$
stiffness:	$c_p = 1 \cdot 10^{11}$ N/m				

contact

sector:	$\varphi_0 = \arctan(L_p/(2R))$ c.o.f.: $\mu = 0.4$
mean pressure:	$p_0 = 1000\text{N}/(L_p b_p)$
contact stiffn.:	$c_N = 3 \cdot 10^{10}$ Pa/m

REFERENCES

[1] H. Hetzler. *Zur Stabilität von Systemen bewegter Kontinua mit Gleitkontakten am Beispiel des Bremsenquietschens*. Dissertation, Fakultät für Maschinenbau, Universitätsverlag Karlsruhe, 2008.

[2] K. Huseyin. *Vibrations and Stability of Multiple Parameter Systems*. Springer-Verlag, 1978.

[3] RA Ibrahim. Friction-induced vibration, chatter, squeal and, chaos; Part I: Mechanics of contact and friction. *ASME Applied Mechanics Reviews*, 47(7):209–226, 1994.

[4] K.L. Johnson. *Contact mechanics*. Cambridge University Press, 1987.

[5] Inc Karlsson & Sorenson Hibbitt. *ABAQUS/Explicit: Example Problems Manual (Version 6.1.): Brake squeal analysis*. Hibbitt, Karlsson & Sorenson, Inc, 2000.

[6] O.N. Kirillov. On the stability of nonconservative systems with small dissipation. *Journal of Mathematical Sciences*, 145(5):5260–5270, 2007.

[7] D.B. McIver. Hamilton's principle for systems of changing mass. *Journal of Engineering Mathematics*, 7(3), 1973.

[8] M.R. North. Disc brake squeal. In *Proc. Conf. on Brake of Road Vehicles, C*, volume 38, 1972.

[9] A.P. Seyranian and A.A. Mailybaev. *Multiparameter stability theory with mechanical applications*. World Scientific, 2003.

[10] H.A. Sherif. Investigation on effect of surface topography of pad/disc assembly on squeal generation. *Wear*, 257(7-8):687–695, 2004.

[11] H. Storck and F. Moser. Two dimensional friction force in brake squeal. *Braking 2004: Vehicle Braking and Chassis Control*, 2004.

[12] H. Ziegler. *Principles of Structural Stability*. Birhäuser Verlag, 1977.